The short-range order in some ternary ZrF_4-based glasses

1994 J. Phys.: Condens. Matter 6 2159

(http://iopscience.iop.org/0953-8984/6/11/005)

J. Phys.: Condens. Matter 6 (1994) 2159–2168. Printed in the UK

The short-range order in some ternary ZrF_4-based glasses

Wen-cai Wang†, Yu Chen† and Tian-dou Hu‡

† Department of Physics, Peking University, Beijing 100871, People's Republic of China
‡ Beijing Electron Positron Collider National Laboratory, Beijing 100039, People's Republic of China

Received 20 July 1993, in final form 8 November 1993

Abstract. The short-range order structures in some ternary ZrF_4–BaF_2-based glasses doped with EuF_3, AlF_3 or NaF are studied by XAFS. The near-neighbour structures around Zr, Ba and Eu are determined and compared with that in binary ZrF_4–BaF_2 glasses. The structural parameters of near neighbours around Zr and Ba are slightly reduced on addition of NaF or AlF_3. Also, it is observed that the intensities of the 'white lines' in the L_n and L_m absorption edges of Eu and Ba in these glasses are different from those in corresponding fluorides. The causes leading to these changes are discussed. Meanwhile the differences between the bonding behaviour of Eu–F and that of Ba–F in the glasses are also discussed.

1. Introduction

Many studies have been made on fluoride glasses since it was first reported. The technical applications and potentiality of these glasses has stimulated the development of new materials and investigations of their properties [1, 2]. However, in comparison, there have still not been many structural studies and more attention should be paid to these [2–4].

Although ZrF_4–BaF_2-based glasses have been extensively investigated, the reports on their structures have been mainly limited to binary and a few ternary glasses. The results on the local structures around Zr have not been consistent with each other [4–6]. With the selective characteristics of the x-ray absorption spectrum (XAS), we can analyse the local structures around every metal cation in ZrF_4–BaF_2–EuF_3 glasses. EuF_3 is one of the components in some multicomponent ZrF_4-based glasses [7, 8]. The Eu ion has been shown to have mixed valence states in some compounds [9, 10]. Therefore, the Eu valence behaviour and bonding characteristics between Eu and F in the glasses should be interesting. Also, AlF_3 and NaF are important components in ZrF_4–BaF_2-based glasses. Their structural effects also need to be investigated.

As is well known, 'white lines' (WLs) occur at the Ba and Eu $L_{n,m}$ edges and these WLs have been attributed to the electronic transition from a 2p to a 5d state. The Ba atom has an electronic configuration (Xe) $6s^2$, and Eu has the configuration (Xe) $4f^7 6s^2$. Their 5d states are not occupied and the 5d band is very narrow in Ba and Eu as well as in their compounds, so that a WL appears [11].

Investigations on the intensities of the $L_{n,m}$-edge WLs from heavier 4d transition metals (TMs), 5d TMs and their compounds [12–14] showed that these WL intensities were determined by the population of the d band except for the first two 5d elements. The intensities of the $L_{n,m}$ WLs decreased with increasing atomic order number of these elements, while their d bands were occupied gradually. However, the intensities decreased anomalously with decreasing atomic number from Ta to Hf to Lu. This anomaly was

0953-8984/94/112159+10$19.50

considered to be a relaxation effect related to the creation of a 2p hole. The core–hole effect would dominate in lighter 5d elements.

Otherwise, the intensity ratio of L_m to L_n should have a statistical value of 2 to 1, because the L_n and L_m absorption spectra are assigned to a dipole-allowed transition of an electron from $2p_{1/2}$ to $d_{3/2}$ and from $2p_{3/2}$ to $d_{3/2}$, $d_{5/2}$, respectively. This has been proved by many studies [12, 14, 15], but it has been reported that the ratios deviated significantly from the statistical distribution in some situations, e.g. for Na [16], for 3d TMs [17] and for the d band of a metal which is nearly full [12, 14]. These related to the behaviour of the electronic configuration of a material.

In this paper, we studied four glasses including three ternary fluoride glasses by x-ray absorption fine structure (XAFS). Their local structures surrounding Zr, Ba and Eu were determined and compared with those in binary ZrF_4–BaF_2 glasses. We discussed the structural differences in the glasses containing various third components in the glasses. In terms of the changes in the $L_{n,m}$-edge WLs, the bonding characteristics between metal cations and fluorine were also discussed.

2. Experiment

The glasses used in this investigation were prepared by a melt of mixed fluoride powders and quenching at a higher cooling rate in a flow of dry nitrogen gas.

Samples for XAFS measurement were prepared by making fine powders of materials (400 mesh) dispersed onto a polymer transparent tape homogeneously. The sample was made of a few layers of this tape to obtain the optimum thickness.

X-ray absorption spectra were measured in transmission mode at the extended x-ray absorption fine-structure (EXAFS) station of synchrotron radiation in the Beijing Electron Positron Collider National Laboratory (BEPC NL). At 2.2 GeV energy and an injection current from 20 to 40 mA in the storage ring, the Eu and Ba $L_{n,m}$-edge x-ray absorption spectra were taken with a Si(111) double-crystal monochromator and the detector of two ion chambers. The smallest scanning step was 1 eV.

The ratio of N_2 to Ar in the first ion chamber was adjusted properly so that the intensity of the incident x-ray decreased by about 20% after transmission. Care was taken to suppress the high harmonics by slightly detuning the monochromator.

The Zr K-edge spectra were obtained using a Rigaku model RU-200 rotating-anode x-ray generator and Rigaku EXAFS spectrometer with a Rowland circle radius of 320 mm. The generator was run at 27 kV and 40 mA. The spectra were measured with a Si(220) Johansson bent-crystal monochromator in transmission mode with the sample moving in or out of the beam at every measured energy. The detector was a scintillation counter and the smallest scanning step was 2 eV. When measuring an absorption spectrum, we used a divergence slit of 1° and receiving slits of 0.2 mm (horizontal) and 10 mm (vertical). The measuring time was 20 s at every data point. When the maximum I_0 was not higher than 4×10^4 s^{-1} (the top limit of the linear range of measured intensity) in the whole wave band of a measured spectrum, the minimum number of intensity counts still reached $n \times 10^4$. Hence, the statistical error in the counts of beam intensities was less than 1%.

We measured Zr K and Ba $L_{n,m}$-edge x-ray spectra in four glasses ZBEu4 ($56ZrF_4$–$40BaF_2$–$4EuF_3$), ZBEu8 ($62ZrF_4$–$30BaF_2$–$8EuF_3$), ZBN ($56ZrF_4$–$40BaF_2$–$4NaF$) and ZBA ($56ZrF_4$–$40BaF_2$–$4AlF_3$) as well as Eu $L_{n,m}$-edge spectra in the glasses containing EuF_3. These spectra were also measured under the same experimental conditions for the crystalline compounds K_2ZrF_6, Li_2ZrF_6, BaF_2 and EuF_3 as reference compounds.

3. Data analyses and main results

Data analyses used a general processing procedure [18]. First, the EXAFS function $\chi(k)$, where k is the wavenumber of the photoelectron, was extracted by pre-edge and post-edge background removal and normalization. Figure 1 shows Eu L_m-edge absorption spectra for c-EuF_3 and for ZBEu4 and ZBEu8 glasses after pre-edge background removal. Then the radial structural function (RSF) was obtained by Fourier transformation of $k^n\chi(k)$, where n is equal to 3 for the K edge and equal to 1 for the L edge. The RSFs around Eu in several materials are shown in figure 2. Finally, the $\chi_l(k)$ corresponding to the EXAFS contribution from the near-neighbour coordination shell was extracted by inverse Fourier transformation of the first peak in a RSF. The near-neighbour structural parameters were determined by the curve-fitting method in terms of the following formula [18]:

$$\chi_l(k) = \sum_j \frac{N_j F_j(r,k)}{kr_j^2} \exp\left(\frac{-2r_j}{\lambda}\right) \exp(-2k^2\sigma_j^2) \sin[2k\gamma_j + \psi_j(r,k)]$$

where j is the number of indistinguishable subshells in the near-neighbour coordination shell, in which there are N_j coordination atoms in the jth subshell at the mean distance r_j. σ_j^2 is the mean square deviation between the central atom and atoms of the jth subshell. λ denotes the average free path of photoelectrons. $F_j(r,k)$ and $\psi_j(r,k)$ are the back-scattering amplitude per atom and phase shift function respectively, for the jth shell.

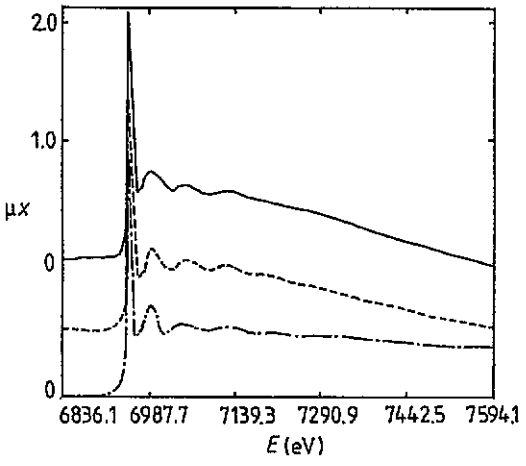

Figure 1. Eu L_m-edge x-ray absorption spectra in several materials: — · —, c-EuF_3; – – –, g-ZBEu4; ——, g-ZBEu8.

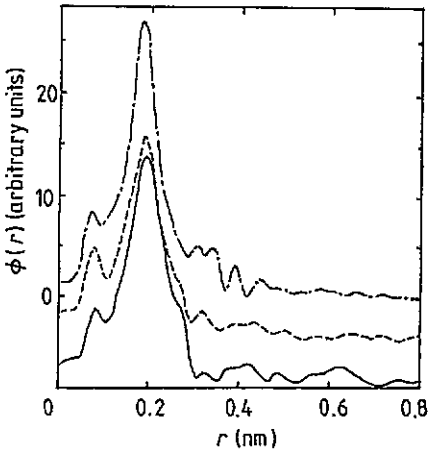

Figure 2. Radial structural functions $\phi(r)$ around Eu in some materials: — · —, c-EuF_3; – – –, g-ZBEu4; ——, g-ZBEu8.

To determine the near-neighbour structural parameters around Zr in four glasses, we used two reference compounds, which have different near-neighbour coordination numbers: 6 and 8. $F(r,k)$ and $\psi(r,k)$ were obtained in two ways. First they were extracted from the experimental data of reference compounds; secondly the values were theoretically calculated by the FEFF 3.11 program package [19]. In the FEFF 3.11 program package, $F(r,k)$ and $\psi(r,k)$ were calculated using an approximate distance of the atom pair concerned, while the values obtained from reference compounds correspond to a definite shell, which includes the effect

of the distance r. The structural parameters were obtained by curve fitting with the $F(r,k)$ and $\psi(r,k)$ functions. The results obtained from different amplitude and phase functions were close to each other. Their average values gave the final results. In table 1 the values for the reference compounds are the results from fitting with theoretical functions, while the values in parentheses are structural data determined by diffraction [20, 21].

Table 1. Near-neighbour structural parameters around Zr.

Sample	N	r (nm)	$\Delta\sigma^2$ (10^{-5} nm^2)
K_2ZrF_6	7.7 ± 0.4 (8)	0.211 ± 0.001 (0.2114)	5.3 ± 0.4
Li_2ZrF_6	5.8 ± 0.3 (6)	0.202 ± 0.001 (0.2016)	4.6 ± 0.3
g-ZBEu4	7.1 ± 0.4	0.207 ± 0.002	5.9 ± 0.4
g-ZBEu8	7.2 ± 0.3	0.206 ± 0.002	6.3 ± 0.3
g-ZBN	6.6 ± 0.4	0.204 ± 0.002	5.7 ± 0.4
g-ZBA	6.5 ± 0.4	0.204 ± 0.002	6.2 ± 0.3

When determining the local structures around Eu in the glasses, $F(r,k)$ and $\psi(r,k)$ cannot be extracted from the experimental data of EuF_3 because the near neighbours around Eu include five subshells in EuF_3. However, EuF_3 can be used to verify the appropriateness of the functions theoretically calculated. To reduce the numbers of fitting parameters, five near Zr–F distances were regrouped in three sets. The results are listed in table 2, where the values in parentheses are the reported structural data [22]. Figure 3 shows the experimental (full curve) and fitted curve (dotted curve) of $k\chi_I(k)$ corresponding to Eu in ZBEu8 glass.

Table 2. Near-neighbour structural parameters around Eu.

Sample	N	r (nm)	$\Delta\sigma^2$ (10^{-5}nm^2)
EuF_3	6.6 ± 0.4 (7)	0.237 ± 0.002 (0.2360)	3.1 ± 0.4
	1.9 ± 0.3 (2)	0.254 ± 0.001 (0.2538)	4.6 ± 0.3
	2.0 ± 0.4 (2)	0.288 ± 0.002 (0.2886)	4.9 ± 0.5
g-ZBEu4	7.1 ± 0.4	0.228 ± 0.003	6.7 ± 0.4
	3.4 ± 0.5	0.273 ± 0.004	6.3 ± 0.5
g-ZBEu8	7.2 ± 0.4	0.229 ± 0.003	5.7 ± 0.4
	3.2 ± 0.4	0.275 ± 0.003	6.2 ± 0.4

The near-neighbour structural parameters of Ba may not be accurate because of the small range of data (the energy range of the Ba L_m-edge absorption spectra is only about 350 eV) and the wider F distribution surrounding Ba. However, as the conditions of experimental and data processing were all the same, the differences in the near-neighbour structures around Ba in various materials can be compared.

Also, we processed the data from the XANES spectra of Eu and Ba $L_{n,m}$ edges. The intensity of each WL was normalized to the edge jump, which was calculated as the difference between the extrapolated values of the pre-edge and post-edge background at the edge. The lineshape of a WL can be approximated by a Lorentzian and the $\tan^{-1}$ function describes the transition into the continuum states [11, 23]. So, after normalization, the edge was fitted with the superposition of a Lorentzian line (to model the WL) and a $\tan^{-1}$ function (to model the continuum absorption). Therefore, the intensities of various WLs in different materials

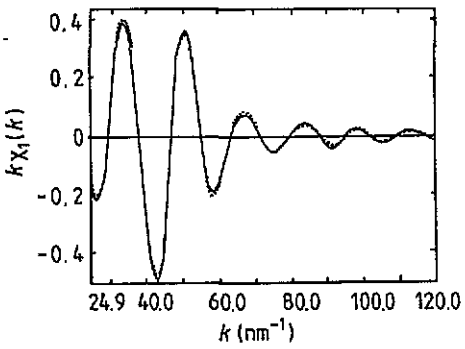

Figure 3. $k\chi_1(k)$ corresponding to near neighbours around Eu in g-ZBEu8: ——, experimental; ·····, fitted curve.

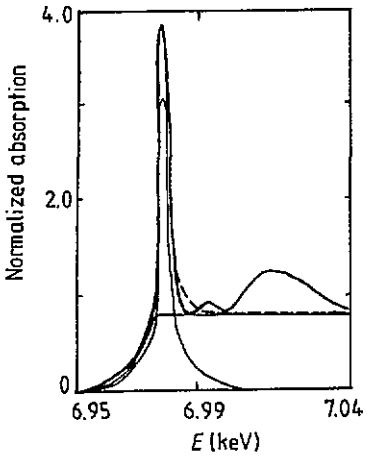

Figure 4. Eu L_m edge (——) and fitted curve (——, – – –) in ZBEu8.

can be compared using the height or the area under a Lorentzian peak. Figure 4 gives the experimental Eu L_m edge (full curve) and fitted curve (thin full and broken curves) in ZBEu8. Figure 5 represents the normalized intensities of Eu$L_{n,m}$-edge WLs in ZBEu4 and ZBEu8 glasses and c-EuF_3. The Ba L_n and L_m edges of c-BaF_2, g-ZBEu4 and g-ZBN are shown in figures 6(*a*)–(*c*), respectively.

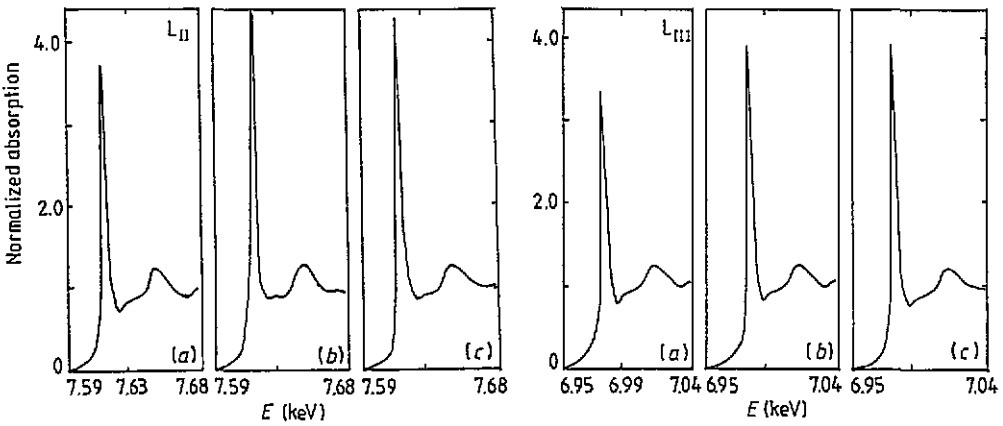

Figure 5. Normalized intensities of the WLs of the Eu L_n and L_m edges in (*a*) c-EuF_3, (*b*) g-ZBEu4 and (*c*) g-ZBEu8.

Table 3 lists the comparison of the WL intensities of the Eu $L_{n,m}$ edges and the intensity ratios of L_m to L_n for ZBEu4, ZBEu8 and c-EuF_3, and of the Ba $L_{n,m}$ edges of the studied glasses and c-BaF_2 are given in table 5.

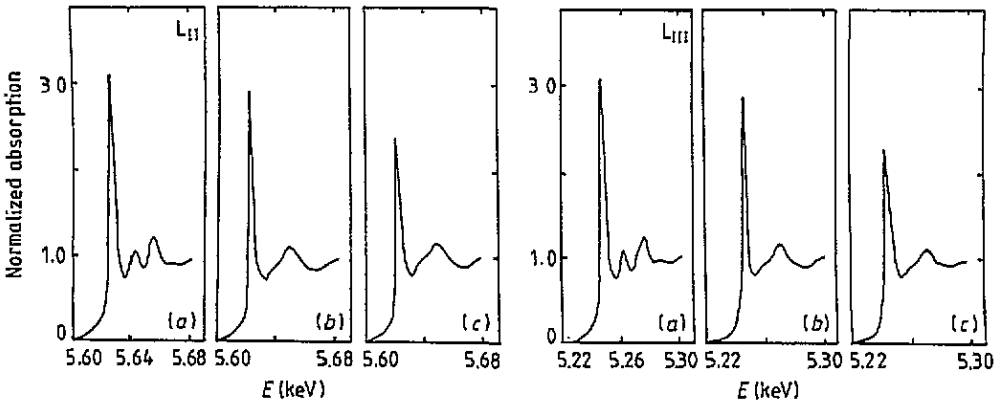

Figure 6. Normalized intensities of the WLS of the Ba L_n and L_m edges in (*a*) c-BaF_2, (*b*) g-ZBEu4 and (*c*) g-ZBN.

Table 3. The relative intensities and the L_m to L_n intensity ratio of WLS at the Eu $L_{n,m}$ edges.

Eu WL	L_m		L_n		L_m to L_n ratio	
sample	Height	Area	Height	Area	Height	Area
EuF_3	1.00	1.00	1.00	1.00	0.89	0.87
ZBEu4	1.22	1.21	1.24	1.27	0.85	0.83
ZBEu8	1.20	1.20	1.24	1.27	0.84	0.82

4. Discussion

4.1. Near-neighbour structure around Zr

The results on the near-neighbour coordination number around Zr that have been reported by some workers for ZrF_4–BaF_2 and a few ternary ZrF_4-based glasses are not consistent. For the most extensively studied glass $2ZrF_4$–BaF_2, different values of the coordination were reported, for instance, sixfold coordination [4] was obtained by vibrational spectra, eightfold coordination [6] was determined by Raman spectra and seven to eight neighbours were found by x-ray scattering [5].

As shown in table 1, we obtained a near-neighbour coordination number around Zr of approximately 7 in the glasses studied. The mean distance between Zr and the nearest F neighbours was about 0.206 ± 0.002 nm. In the glasses doped with AlF_3 or NaF, these two parameters were slightly reduced, compared with ZBEu4, ZBEu8 and binary ZrF_4–BaF_2 glasses [24]. Although these changes were apparently within errors of measurement, the comparison between the data of various materials may be more accurate than the data themselves as they were obtained in the same experimental and data-processing conditions. The reasons for this reduction are discussed later.

In the RSFs around Zr of four glasses, there were second peaks with small amplitudes at approximately the same position. These peaks were too small for data processing to be carried out accurately. We identified the back-scattering atoms corresponding to them by the amplitude- and phase-corrected Fourier transformation (APCFT) [24]. According to the coincidence of peak positions between the magnitude and imaginary part of APCFT [18], these peaks may correspond to Zr–Zr and Zr–Ba distributions. The estimated values of the

Zr–Zr mean distance are 0.36 ± 0.1 nm. This distance is consistent with that of the co-edge bipolyhedra Zr_2F_{13} existing in $2ZrF_4$–BaF_2 glass [25]. Therefore, the Zr–Zr interaction by edge sharing may exist in ZrF_4-based glasses.

In brief, the near-neighbour coordination number around Zr was about 7 in ZrF_4–BaF_2-based glasses, where the BaF_2 content was less than 40 mol%. On the basis of this, we believe that sixfold, sevenfold and eightfold polyhedra may all exist. There may be a majority of one type and there may also be bipolyhedra in a glass. The proportion of these different polyhedra will change with various components of glasses. It will be difficult to determine the ratio value of a polyhedron only from EXAFS. The addition of AlF_3 or NaF will reduce the mean distance and coordination number of near neighbours around Zr a little.

4.2. The local environment of Ba

Our results indicated that the F distribution around Ba was over a wider range, so that it gave a wide peak in the RSF. They formed two subshells, i.e., about seven to eight F ions located at 0.26 nm and about three F at 0.3 nm. Table 4 lists the results for four glasses, where the values of BaF_2 given in parentheses are the known structural data [26]. These are near to the result reported by Coupé *et al* [5]. The addition of NaF slightly decreased the coordination number of near neighbours around Ba.

Table 4. Local environment around Ba.

Sample	N	r (nm)	$\Delta\sigma^2$ (10^{-5} nm^2)
BaF_2	8.1 ± 0.3 (8)	0.264 ± 0.003 (0.268)	2.6 ± 0.4
g-ZBEu4	7.8 ± 0.3	0.256 ± 0.003	7.8 ± 0.4
	2.6 ± 0.4	0.297 ± 0.004	7.5 ± 0.6
g-ZBEu8	7.7 ± 0.3	0.258 ± 0.003	7.6 ± 0.5
	2.4 ± 0.4	0.304 ± 0.005	6.9 ± 0.4
g-ZBN	6.6 ± 0.4	0.256 ± 0.003	5.2 ± 0.4
	3.2 ± 0.3	0.289 ± 0.004	4.6 ± 0.3
g-ZBA	7.6 ± 0.3	0.259 ± 0.003	6.5 ± 0.4
	2.5 ± 0.4	0.301 ± 0.004	4.9 ± 0.4

Next we discuss the bonding behaviour between Ba and F in the glasses.

Ba was bonded in large ionicity in our glasses. There was a chemical shift of about 2 eV in the Ba L_n and L_m-edge XANES spectra of these glasses in comparison with the edge energy of pure Ba [27]. This is the same as in the case of the ionic compound BaF_2.

Otherwise, the intensities of Ba $L_{n,m}$ WLs in our glasses were all less than that in BaF_2 as listed in table 5. We suppose that this is because the 5d empty-state density is altered. First, their intensities are determined by the probability of the electronic transition from 2p to 5d and the density of empty 5d states [23]. The probabilities of electronic transition in measured materials are similar to each other as the inner electron configurations of Ba ions are similar. Therefore, the WL intensities of the Ba $L_{n,m}$ edges would be mainly determined by the number of empty 5d states in these materials. Second, for Ba, the 4f orbital lies in the outer position and has a mean radius of about $17a_0$, where a_0 is the Bohr radius [28]. So bonding electronic states in Ba compounds would be Ba 5d states, where there may be hybridization between Ba 5d and ligand outer electronic states. When this hybridization is increased, the density of Ba 5d empty states would decrease and then WL intensities of the

Table 5. The relative intensities and the L_m to L_n intensity ratio of WLs at the Ba $L_{n,m}$ edges.

Ba WL sample	L_m		L_n		L_m to L_n ratio	
	Height	Area	Height	Area	Height	Area
BaF_2	1.00	1.00	1.00	1.00	1.04	1.02
ZBEu4	0.87	0.82	0.90	0.84	0.87	0.85
ZBEu8	0.88	0.81	0.89	0.84	0.88	0.86
ZBN	0.55	0.53	0.64	0.62	0.71	0.69
ZBA	0.78	0.72	0.84	0.79	0.81	0.78

Ba $L_{n,m}$ edge would also be reduced. The lower WL intensities of the Ba $L_{n,m}$ edges suggest stronger hybridization between the Ba 5d and the 2p states of ligand F in the glasses.

As mentioned above, the additional of NaF to ZrF_4-based glass changed in the near-neighbour structures around Zr and Ba and also reduced the WL intensities of the Ba $L_{n,m}$ edges more than in BaF_2. Also, some studies have revealed that Na cations play a structural role similar to that of Ba ions [29, 30], but their effects on the short-range order structures of Zr are not the same. NaF can impede the degree of fluorine ion transport in fluoride glasses [30]. So there may be clusters consisting of Na and fluorine ions in glasses containing NaF. In this way, the F coordination number surrounding Zr and Ba will decrease. It is consistent with a stronger interaction between Ba and F in the glasses to which NaF has been added.

Finally, we discuss the anomalous L_m-to-L_n intensity ratios at the Ba L_n and L_m edges. The theory given by Wendin [31] explained the non-statistical intensity ratio of a WL resonance. As shown by the theory, the statistical weighting of spin–orbit-split subshell cross sections would be affected by an electron–hole exchange interaction. The statistical weight would be valid only for situations where the spin–orbit splitting of the binding energy is much larger than the exchange interaction. The exchange interaction would result in a reduction in the oscillator strength of the subshell with the lower binding energy ($j = l + \frac{1}{2}$) and an increase in the oscillator strength for higher binding energies ($j = l - \frac{1}{2}$). In the Δ/λ ranges from 0.5 to 5, where Δ denotes the spin–orbit interaction energy and λ is the exchange interaction, the peak intensities corresponding to $j = l + \frac{1}{2}$ become stronger with increasing Δ/λ even though the intensity ratios still deviated from the statistical value. For the $L_{n,m}$ edges of Na, a deviation in the intensity ratio from the statistical value of 2 to 1 was also observed and was explained in terms of the relation of the electron–hole exchange interaction to the spin–orbit splitting [16].

We observed that the L_m-to-L_n intensity ratios were all non-statistical in the glasses studied and in BaF_2 and the deviation from the statistical value for the glasses was larger than for BaF_2. The Ba $L_{n,m}$ edges are due to deep-level excitation in a heavier element; at first glance, the 2p hole–5d electron exchange interaction seems to be much less than the spin–orbit splitting interaction. We suppose that some changes in electronic configurations in the glasses and fluoride may cause an exchange interaction other than the electronic transition from 2p to 5d. The origin of this interaction needs to be further studied.

4.3. The near-neighbour structure around Eu

Table 2 lists the near-neighbour structures around Eu in ZBEu4, ZBEu8 and EuF_3, where the values in parentheses give the reported data [22]. The five subshells of near neighbours around Eu in EuF_3 were regrouped as three distances of Eu–F pairs when carrying out the curve fitting, while the best results can be obtained only with two subshells for ZBEu4 and ZBEu8 glasses. Moreover, the nearest Eu–F distances in the glasses were smaller than in

EuF_3. This indicated that the smaller bonding length may be assumed to be Eu–F bridging and the other to be Eu–F non-bridging, which is consistent with considering EuF_3 as a glass intermediate.

EuF_3 is an ionic bonding compound, like other rare-earth fluorides. The Eu ion has been discovered to have a mixed-valence behaviour in some compounds, e.g. $EuPd_3B_x$ ($0 < x \leqslant 1$). Darshan *et al* [9] pointed out that the L_m edges for $EuPd_3B_{0.5}$ and $EuPd_3B$ each showed two distinct peaks separated by about 7 eV. One of these peaks was at the same energy position as that of trivalent Eu in $EuPd_3$. The second peak appeared on the lower-energy side of the Eu^{3+} peak and was assigned to Eu^{2+}. Eu ions had undergone a valence change from Eu^{3+} in pure $EuPd_3$ to a mixed-valence state in $EuPd_3B_x$ ($x = 0.5$ or 1). In our glasses the Eu L_m-edge spectra showed only a single WL peak like that in EuF_3. This suggests that the Eu ions are in a trivalent state in the glasses. But the WL intensities of the Eu L_n and L_m edges in the glasses increased more than that in EuF_3. Also, the L_m-to-L_n intensity ratios deviated from the statistical value of 2 to 1 for the glasses and c-EuF_3, and the deviating values of the former were all larger than those of the latter.

The stronger WL intensities of the Eu $L_{n,m}$ edges can be explained as due to some degree of covalent bonding between Eu and ligands [24]. As the electrons were introduced into the 4f band of Eu^{3+}, the nuclear potential seen from 5d would be screened and the probability of electronic transition from 2p to 5d would increase. Hence, the intensity of the WL would increase but, in terms of smaller changes in the WL intensities, the degrees of covalent bonding in ZBEu4 and ZBEu8 may be a little larger than in EuF_3. Therefore, it would not result in the divalent and/or mixed-valence state of the Eu ion, as proved by the WLs of Eu L_m edges.

Regarding the abnormal L_m-to-L_n intensity ratio at the Eu $L_{n,m}$ edges, we think that the theory of Wendin is appropriate. In comparison, the intensities of the Eu L_n and L_m edges for the glasses and EuF_3 increased because the electrons were introduced into the 4f band of Eu^{3+}. They would screen the nuclear potential seen from 5d; on the other hand, this would increase the interactions between the excited 5d electron and a core hole and also with the 4f electron in the final state of L XAS. So the L_m-to-L_n ratio would deviate more from the statistical value on the glasses.

In short, there is 4f participation in the covalent bonding of ZrF_4-based glasses containing EuF_3. The hybridization strength of Eu 4f and ligands may be less.

5. Conclusion

The addition of less NaF or AlF_3 slightly decreases the mean distance and coordination number of near neighbours around Zr in comparison with that in ZrF_4–BaF_2-based binary glasses and glasses containing EuF_3. NaF also reduces the coordination number around Ba slightly.

The intensities of Ba $L_{n,m}$ WLs in some ZrF_4–BaF_2-based glasses are all less than in BaF_2 while those of Eu $L_{n,m}$ WLs in ZBEu4 and ZBEu8 glasses are larger than in EuF_3. The L_m-to-L_n intensity ratios of Ba and Eu WLs are all non-statistical in the glasses and fluorides studied. Moreover, for the Eu and Ba L edges the deviations of the intensity ratio from the statistical value in the glasses are larger than in the corresponding fluoride. There are some degrees of covalent bonding between Eu and F in the glasses doped with EuF_3. Otherwise, there may be stronger interaction between Ba 5d and F 2p in the glasses studied.

Acknowledgments

The authors would like to thank Yu-Ying Chen and Jian An of the Beijing Glass Research Institute for making the glasses studied. They are also grateful for the experimental opportunity at BSRF. This work was supported by National Nature Science Foundation of China and was partially supported by BEPC NL.

References

[1] Poulain M 1983 *J. Non-Cryst. Solids* **56** 1
[2] Lucas J 1986 *J. Non-Cryst. Solids* **80** 83
[3] Mosel G and Blau W 1990 *Amorphous Structures: Methods and Results* ed D Schulze (Berlin: Akademie) pp 126–9
[4] Almeida R M and Mackenzie J D 1981 *J. Chem. Phys.* **74** 5954
[5] Coupé R, Louër D, Lucas J and Léonard A J 1983 *J. Am. Ceram. Soc.* **66** 523
[6] Kawamoto Y 1984 *Phys. Chem. Glasses* **25** 88
[7] Coey J M D, McEvoy A and Shafer M W 1981 *J. Non-Cryst. Solids* **43** 387
[8] Samek L, Wasylak J and Marczuch K 1992 *J. Non-Cryst. Solids* **140** 243
[9] Darshan B, Padalia B D, Nagarajan R, Dhar S K, Malik S K and Vijayaraghavan R 1984 *Phys. Rev.* B **30** 4031
[10] Sampathkumaran E V, Kaindl G, Krone W, Perscheid B and Vijayaraghavan R 1985 *Phys. Rev. Lett.* **54** 1067
[11] Jhans H and Croft M 1985 *J. Magn. Magn. Mater.* **47–8** 203
[12] Sham T K 1985 *Phys. Rev.* B **31** 1888
[13] Sham T K 1985 *Phys. Rev.* B **31** 1903
[14] Boyun Qi, Perez I, Ansari P H, Lu F and Croft M 1987 *Phys. Rev.* B **36** 2972
[15] Bainconi A, Modesti S, Campagna M, Fisher K and Stizza S 1981 *J. Phys. C: Solid State Phys.* **14** 4737
[16] Onodera Y 1975 *J. Phys. Soc. Japan* **39** 1482
[17] Leapman R D, Grunes L A and Fejes P L 1982 *Phys. Rev.* B **26** 614
[18] Lee P A, Citrin P H, Eisenberger P and Kincaid B M 1981 *Rev. Mod. Phys.* **53** 769
[19] Rehr J J, Mustre de Leon J, Zabinsky S I and Albers R C 1991 *J. Am. Chem. Soc.* **113** 5135
[20] Hoppe V R and Mehlhorn B 1976 *Z. Anorg. Allg. Chem.* **425** 200
[21] Brunton G 1973 *Acta Crystallogr.* B **29** 2294
[22] Hellwege K-H and Hellwege A M (ed) 1973 *Landolt–Börnstein New Series* Group 3, vol 7a (Berlin: Springer) p 34
[23] Bianconi A, Garcia J and Banfatto M 1988 *Topics in Current Chemistry* vol 145 (Berlin: Springer) p 29
[24] Wen-cai Wang, Yu Chen and Tian-dou Hu 1993 *J. Non-Cryst. Solids* **152** 172
[25] Phifer C C, Angell C A, Laval J P and Lucas J 1987 *J. Non-Cryst. Solids* **94** 315
[26] Muhll R, Andersson S and Galy J 1971 *Acta Crystallogr.* B **27** 2345
[27] Bearden J A and Burr A F 1967 *Rev. Mod. Phys.* **39** 125
[28] Lucatorto T B, McIlrath T J, Hill III W T and Clark C W 1982 *X-ray and Atomic Inner-Shell Physics* ed B Crasemann (New York: American Institute of Physics) p 584
[29] Baldwin C M, Almeida R M and Mackenzie J D 1981 *J. Non-Cryst. Solids* **43** 309
[30] Bray P J, Hintenlang D E, Mulkern R V, Greenbaum S G, Tran D C and Drexhage M 1983 *J. Non-Cryst. Solids* **56** 27
[31] Wendin G 1984 *Phys. Rev. Lett.* **53** 724